Appeared In: *Estuarine and Coastal Modeling, Proceedings of the Seventh International Conference*, M.L. Spaulding and K. Bedford (eds.), American Society of Civil Engineers, pp. 103-119, 2002

A Preliminary Look at Methods to Compute Baroclinic Pressure Gradients in FE Models

Kendra M. Dresback[1], Cheryl Ann Blain[2], and Randall L. Kolar[1]

Abstract

In shelf regions with steep bathymetry in the presence of density gradients, the computation of the baroclinic pressure gradient term in 3D shallow water models may either become unstable or physically unrealistic. This manuscript examines four algorithms to compute the baroclinic pressure gradient term in finite element models. Two common systems for discretizing the vertical are sigma or z-level coordinates. In turn, permutations of these two coordinate systems serve as the basis for the four different algorithms examined herein. All are implemented in the context of the finite element hydrodynamic model, ADCIRC. Several density gradients that vary horizontally and vertically, with the pycnocline occurring at different depths, are used to evaluate the methods in a three-dimensional box grid with variable bathymetry. Initial testing, the subject of this work, focuses on model behavior for simplified problem with known analytic solutions. Long term goals for this study (the subject of subsequent papers) are three-fold: 1) to determine the vertical node placement algorithm that produces the most stable and physically realistic results; 2) to determine the interplay of vertical and horizontal resolution (and bathymetry and density profile), while considering simulation time; and 3) to produce accurate 3D flow fields and baroclinic pressure gradients. Outcomes from the study will be used to direct on-going modeling research in the Mississippi Sound.

Introduction

Background

An accurate prediction of tides and circulation patterns using hydrodynamic models is useful in a wide variety of civilian and military applications that range

1. School of Civil Engineering and Environmental Science, 202 W. Boyd, Room 334, University of Oklahoma, Norman, OK, 73019, USA, dresback@ou.edu, kolar@ou.edu
2. Oceanography Division, Code 7322, Naval Research Laboratory, Stennis Space Center, MS, 39529, USA, blain@nrlssc.navy.mil

from forecasting storm surges from extreme events, such as tsunamis and hurricanes, in order to plan development in coastal areas to predicting circulation patterns in order to guide fleet operations. Moreover, the accuracy of water quality models depends heavily on an accurate, robust hydrodynamic model. One class of models that finds frequent use for these and other applications are the so-called shallow water models.

Shallow water equations in 2D are obtained by vertically averaging the mass and momentum balances over the depth of the fluid. For our applications, we solve the equations using algorithms amenable to irregular triangular meshes (e.g., finite element, finite volume). Such a meshing technique allows grids to be easily refined in shallow coastal areas or in areas with changing topography where high resolution is needed to accurately resolve tidal constituents and circulation patterns. Also irregular coastal boundaries are more accurately described with triangular elements, and flux-type boundary conditions enter the problem naturally. Models in this class include ADCIRC [16], QUODDY [22], and UTBEST [5]. Finite difference based models, such as SIMSYS2D[15], CH3D [4], and POM [30] that use a staggered grid on an orthogonal curvilinear mesh, are stable and mass conservative, but their grids are not as inherently flexible as those based on irregular triangular meshes [15, 29].

Early finite element solutions of the shallow water equations were often plagued by spurious oscillation modes. Various methods were introduced to eliminate the oscillations, but most include some type of artificial or numerical damping [27, 31]. Lynch and Gray [21] present the wave continuity equation as a means to eliminate spurious oscillations without resorting to artificial damping. It is currently the base algorithm in ADCIRC (ADvanced 3D CIRCulation model [16]), the model that is the subject of this research.

Since the inception of the wave continuity formulation in 1979, the original algorithm has been modified in a number of substantial ways: Kinnmark introduced a numerical parameter to provide a general means of weighting the continuity equation [11]; viscous dissipation terms were incorporated [12, 20]; and 3D barotropic simulations were realized by resolving the velocity profile in the vertical [16, 25]. Most recently, the model has incorporated the following features: a wetting/drying algorithm for near-shore elements [17]; spherical coordinates for large domains via a map projection technique [13]; a parallel domain decomposition algorithm for the 2D portion of the code [26]; a fully implicit time marching algorithm [6]; options for hydraulic structures (e.g., levees, breakwaters); and a diagnostic baroclinic algorithm [18]. These advances are all present in the current version of the ADCIRC model, a model that represents over 20 years of research and development by scientists and engineers at six different institutions. ADCIRC has been extensively tested using analytical solutions and field data, and it is being used by a diverse group of researchers and practitioners to model the hydrodynamic behavior of many coastal and oceanic regions [2, 7, 8, 10, 23, 34].

Long-Term Research Objectives

Our long-term research objective is to modify the existing hydrodynamic model, ADCIRC, so that it is capable of 3D prognostic baroclinic simulations on high performance (massively parallel) computing platforms. As a first step toward that objective, we have inaugurated a systematic study to determine the interplay between the level of horizontal and vertical resolution, the type of vertical coordinate system, and bathymetry and density profiles. Several others (e.g. [1, 9]) have examined the impact of the type and/or amount of resolution of vertical coordinates on solution results, but they were done either in the context of finite difference models or a static grid. For example in the framework of a finite element model, Walters and Foreman [32] investigated the effect of horizontal resolution for a fixed vertical resolution (and vice versa) on velocities using sigma coordinates. In their paper, they found that the sigma coordinate system in test cases for a continental shelf region produced either second or first order accurate solutions, depending on the density profile. Lastly, they concluded that sigma coordinates should not be used for the types of problems they studied and should be replaced with either level coordinates or post-processing the density field and using a density gradient. Fortunato and Baptista [9] looked at the vertical placement of nodes in the framework of finite elements for a barotropic tidal model. They found that an efficient placement of the vertical nodes may take care of the strong dependence of errors in the local flow properties, however this is not possible with the z-level and traditional sigma coordinates. They introduced localized sigma coordinates, which allowed for more flexibility in the placement of nodes. This proved to be strong alternative to the traditional uniformly distributed sigma and z-level coordinates. Our aim is to build on their efforts, also using finite element hydrodynamic models, by examining several vertical coordinate systems and looking at the interplay of horizontal and vertical resolution.

This intense focus on the 3D behavior of the code is motivated by anomalous results that were observed by Blain [3] in a baroclinic Arabian Gulf simulations using a wave continuity based FE model. Figure 1 illustrates the problem, where the source of error was identified as unrealistic (and unstable) baroclinic pressure gradients computed by the model in a region of steep bathymetry and density gradients. Hence, our initial efforts have focused on developing a protocol to study computed gradients and the resulting flow field.

Initial Studies

Because of the focus on ADCIRC, in the remainder of this paper we present the theoretical basis of the ADCIRC model, starting with the continuum equations and the method of discretization. We then outline the experimental methods along with results from the numerical experiments. For any long term study such as this, a natural first step is to compare model results for simple problems to known analytical solutions. This initial testing is the focus of this paper. From these results,

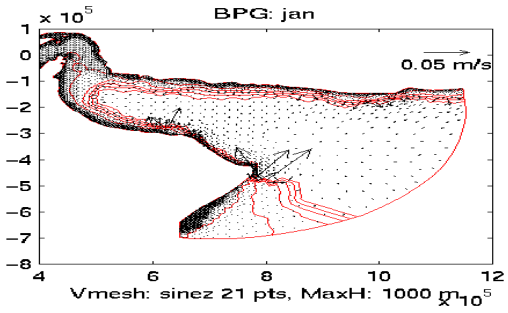

Figure 1. Instabilities (large vectors) caused by errors in the calculation of the baroclinic pressure gradient during simulations of the Arabian Gulf [3].

we can draw some preliminary observations, which help set the stage for future work.

Theoretical Construct - The Conservation Equations

As with nearly all prominent 3D coastal circulation models, ADCIRC uses a mode splitting scheme to solve the 3D balance laws. In this algorithm, which has several variants, the external mode solves the 2D (depth-averaged) continuity equation for the free surface elevation; it is then used to force the internal mode solution of the 3D momentum equations, a step that resolves the 3D structure of the velocity field. The governing equations are summarized below. A full development can be found in the ADCIRC user's manuals [16, 18, 33].

Primitive forms of the 2D balance laws are obtained by vertical averaging of the microscopic balance laws (i.e., those obtained from basic fluid dynamics) over the total fluid depth. With operator notation, the primitive form of the continuity equation, L, is

$$\mathrm{L} \equiv \frac{\partial \zeta}{\partial t} + \nabla \bullet (\mathrm{H}\mathbf{V}) = 0 \tag{1}$$

where ζ is surface elevation above a datum, H is the total fluid depth, and $\mathbf{V}$ is the 2D depth-averaged velocity. The conservative form of the momentum equation, $\mathbf{M}^{\mathrm{c}}$, is given by

$$\mathbf{M}^{\mathrm{c}} \equiv \frac{\partial (\mathrm{H}\mathbf{V})}{\partial t} + \nabla \bullet (\mathrm{H}\mathbf{V}\mathbf{V}) + \mathrm{H}\mathbf{f} \times \mathbf{V} + \mathrm{H}\nabla\left[\frac{p_a}{\rho_0} + g(\zeta - \alpha\eta)\right] - \tag{2}$$
$$\mathbf{K} - \mathbf{D} - \mathbf{B} - \frac{1}{\rho_0}(\mathbf{T}_b - \mathbf{T}_s) = 0$$

where $\mathbf{f}$ is the Coriolis parameter, p_a is the atmospheric pressure at the surface, α is the effective earth elasticity factor, η is the Newtonian equilibrium tidal potential,

ρ_0 is reference fluid density, g is gravity, **K** is the depth-integrated horizontal momentum diffusion, **D** is the momentum dispersion (momentum transfer due to a non-uniform velocity profile), **B** is the depth-integrated baroclinic forcing, $\mathbf{T}_b$ is the bottom stress, and $\mathbf{T}_s$ is the surface stress.

The generalized wave continuity (GWC) equation, is formed from the following operation:

$$\partial L/\partial t + GL - \nabla \cdot \mathbf{M}^c = 0 \tag{3}$$

where G is a numerical parameter. It is used in lieu of (1) to solve for free surface elevation. Note that the wave continuity equation, as it originally appeared in Lynch and Gray [21], is obtained by setting $G = \tau$. Also note that the primitive continuity equation can be viewed as a limiting form of the generalized wave continuity equation by letting $G \to \infty$.

The 3D momentum equations, used by the internal mode solution (after applying the Boussinesq and hydrostatic pressure approximations), are given in non-conservative form by

$$\frac{\partial \mathbf{v}}{\partial t} + \mathbf{v}_{3D} \cdot \nabla \mathbf{v} + \nabla_{xy}\left[\frac{p_a}{\rho_0} + g(\zeta - \alpha\eta)\right] - \frac{\partial}{\partial z}\frac{\tau_z}{\rho_0} - \mathbf{n} + \mathbf{b} = 0 \tag{4}$$

where $\mathbf{v} = (u, v)$, $\mathbf{v}_{3D} = (u, v, w)$, (u, v, w) are the (x, y, z) components of velocity (or East, North, and vertical if spherical coordinates are used), respectively, ∇ is the 3D gradient operator, ∇_{xy} is the 2D gradient operator in the x, y-plane, τ_z is the vertical stress, **n** is the lateral stress gradient, and **b** is the baroclinic pressure gradient given by

$$\mathbf{b} = g\nabla_{xy}\int_{-z}^{\zeta} \frac{(\rho - \rho_0)}{\rho_0} dz \tag{5}$$

Numerical Implementation

Semi-discrete equations are obtained by interpolating the GWC equation with C^0 linear finite elements (triangles). Exact quadrature rules are used throughout. Implicit time discretization of the GWC equation uses a three-time-level approximation centered at k. In 3D, a mode splitting algorithm is used where the GWC (3) is solved for nodal elevations and the 3D momentum equation (4) is solved for the velocity field. The default algorithm in ADCIRC is to compute horizontal gradients in (4) using a level or "z" coordinate system, while the remaining terms are evaluated in a stretched σ-coordinate system. However, alternative methods of computing the baroclinic pressure gradient term (5) are the subject of this article and are discussed in detail below.

Experimental Methods

Because of the problems illustrated in Figure 1, our initial work has focused on analysis of the baroclinic pressure gradient (BPG) term. The literature indicates that the two most common coordinate systems are the sigma (i.e. terrain-following) and z-level (i.e. fixed-depth) [1]. In our study, these coordinate systems are used to define four different methods for calculating the BPG; the methods are summarized in Figure 2 and Table 1. Each coordinate system offers several advantages and

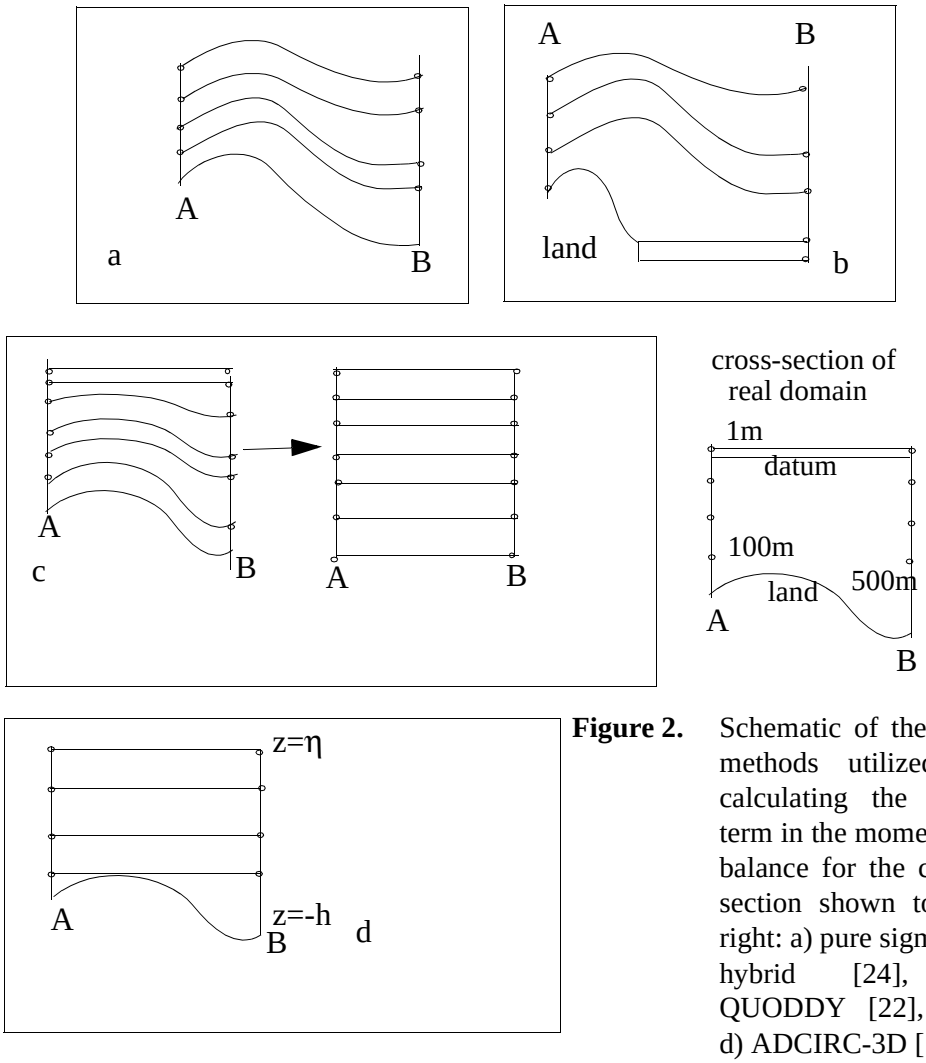

Figure 2. Schematic of the four methods utilized in calculating the BPG term in the momentum balance for the cross-section shown to the right: a) pure sigma, b) hybrid [24], c) QUODDY [22], and d) ADCIRC-3D [18]

disadvantages, both from a numerical implementation perspective and from an accuracy perspective. In particular, z-coordinate systems are good at resolving horizontal gradients, but the “stair-step” bottom slope representation causes inaccuracies in bed stress and advection calculations near the bed, which can lead

Table 1. Description of vertical coordinate systems used for calculating the baroclinic pressure gradient.

Coordinate Systems	Specifics
Sigma	Terrain following. See Figure 2a.
Sigma/z-level	A hybrid sigma/z-level coordinate system that switches methods based on the vertical depth. The sigma coordinates reside on the upper section while the z-level coordinates make up the lower section. See Figure 2b. This method is currently being used in NCOM (Naval Coastal Ocean Model) [24].
Predetermined level surfaces	Used in the QUODDY FE model to compute the BPG term where the predetermined level surfaces often coincide with depths at which the modeler knows the structure of the density field. In this case, there are a uniform number of vertical nodes under every horizontal nodes, which are terrain and free surface following [22]. See figure 2c.
Sigma/z-level	Used in the 3D ADCIRC model. The BPG terms are calculated along level coordinates. See Figure 2d. For other terms in the momentum equation, a generalized stretched vertical coordinate is used where the z-level coordinates are transformed to variable sigma coordinates (where σ_b=-1 and σ_a=1). This represents a stretched sigma coordinate method, but it allows for the nodes to be distributed vertically in any manner [18].

to artificial cross diffusion. On the other hand, the σ-coordinate system can follow the bottom topography, but can lead to large truncation errors when computing horizontal gradients around the pycnocline [1]. Hence the appearance of hybrid methods that take advantage of each method's strengths. To isolate the impact of the BPG on the resulting velocity field, we import the gradients calculated by any of the four methods into the 3D ADCIRC code, which then computes the velocity field, thus providing a consistent basis for comparing each BPG method (see notes in Table 1). With any vertical grid, one must also consider the distribution of nodes. For the initial study, we are using a uniform distribution; later work will consider sinusoidal and others suggested by the literature.

The domain used for this initial study is an idealized basin, which provides a good check on our numerical algorithms since, for simple density fields, it has an analytic solution. The idealized basin is a 48 km (east-west) x 16 km (north-south) rectangular domain with varying levels of horizontal and vertical resolution. Initially, the horizontal resolution is set at 1000 m, but the vertical resolution can vary. Two bathymetry profiles are considered: 1) a constant 10m or 100m depth ("flat bottom") and 2) a linear variation from 10m at the shallow end to 100m at the

deep end ("sloped bottom" with a constant slope of approximately 0.2%). Boundary conditions on all sides of the ideal basin are land boundaries with no normal flow as natural boundary conditions, but free tangential slip is allowed. Other invariant conditions of the simulation are as follows (exceptions will be noted): horizontal eddy viscosity mixing processes are neglected (negligible horizontal velocity gradients), cold start, 1-day simulation time, no north-south variations in the density field, G in the GWC solution set to 0.01/sec, linear slip bottom condition, and the nonlinear terms turned off except for the bottom friction.

BPG Tests

The density fields for the idealized basin are summarized in Table 2. Density fields were chosen to facilitate the computation of an analytic solution or to be representative of field gradients; they can be grouped into 3 categories: 1) The density only varies in the horizontal (either linearly or quadratically), which lend themselves to a non-zero analytic solution for the baroclinic pressure gradient; 2) The density varies in the vertical direction only (discussed in Table 2, #4 and #5), which has an analytic baroclinic pressure gradient of zero; and 3) A density field that varies both in the vertical and horizontal directions.

In all cases, there is no north-south density variation and the reference density, ρ_0, is constant, so equation (5) simplifies to

$$b_x = g\frac{\partial}{\partial x}\int_{-z}^{\zeta}\frac{(\rho-\rho_0)}{\rho_0}dz = \frac{g}{\rho_0}\int_{-z}^{\zeta}\frac{\partial\rho}{\partial x}\,dz \tag{6}$$

For the first flat bottom case (Table 2, #1) and the first two sloped bottom cases (Table2, #1 and #2), the density does not vary with depth either so (6) further simplifies to

$$b_x = \frac{gz}{\rho_0}\frac{\partial\rho}{\partial x} \tag{7}$$

where ρ is a known function of x and where we have assumed that the elevation set-up is small and can be neglected in the integral (i.e., ζ is set to zero). Numerical tests verified this assumption. For the second flat bottom case, the density field over the vertical is not constant, but it does vary as a known function so that the analytic BPG can be calculated from (6). Such is not the case for the third sloped bottom case, whose density field is shown in Figure 3. For this case, we used an over-

resolved grid in the vertical (101 nodes or levels) to establish the true solution.

Table 2. Density fields used to test BPG calculations[a].

Flat Bottom	Sloped Bottom
1) Linear variation from 1000 (east) to 1036 (west). Constant over 10m depth.	1) Linear variation from 1000 (east) to 1036 (west). Constant over depth.
2) Quadratic increase from 1000 (east) to 1036 (west). Constant over depth.	2) Quadratic increase from 1000 (east) to 1036 (west). Constant over depth.
	3) Linear variation from 1000 at the surface (east) to 1036 at the surface (west). Quadratic decrease from surface value with depth. See Figure 3.
	4) Stratified case where the density above 50m is 1027 and below the density is 1034.
	5) Field-representative density variation in the vertical with a well-mixed warm surface layer underlain by logarithmic increase to deeper colder water (see Fig. 3); no variation in the horizontal. Developed from [28].

a. All density units in kg/m^3

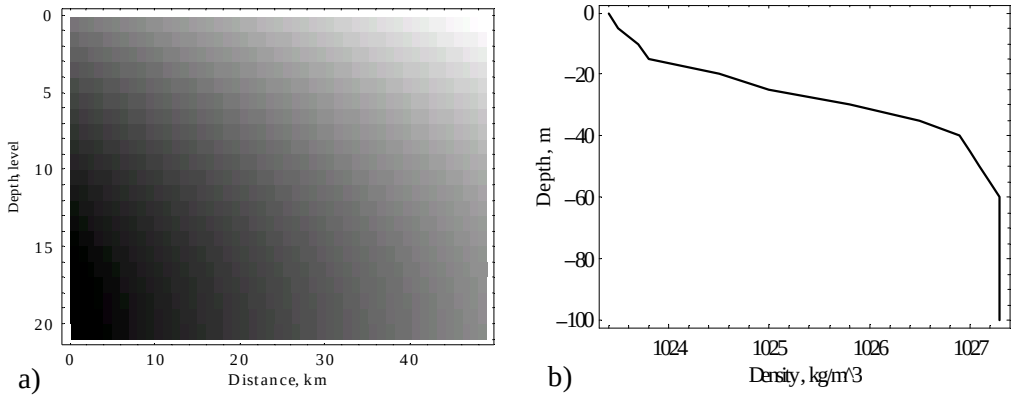

Figure 3. Vertical profiles of the #3 (a) and #5 (b) density fields described in the right column of Table 2. Darker color in the left panel represents lower density.

Velocity Tests

As discussed earlier, BPG results from any of the methods are fed into the 3D ADCIRC model to compute the 3D velocity field. Table 3 summarizes the

vertical experiments and parameter studies with this code for the idealized basin.

Table 3. Velocity experiments and parameter studies.

Flat Bottom[a]	Sloped Bottom[b]
1) Constant vertical eddy viscosity, 10m and 100m depth, linear slip bottom boundary condition.	1) Constant vertical eddy viscosity, linear slip bottom boundary condition.
2) Impact of ramp function when using cold starts.	2) Linear vs. quadratic slip bottom boundary condition
3) Linear slip vs. quadratic slip vs. no slip for the bottom boundary condition.	3) Constant vertical eddy viscosity, linear slip bottom boundary condition; more complex density field.
4) Impact of "G," the numerical parameter in the GWC equation (conditions as in row 1 above).	

a. For the experiments in this column, only the ADCIRC method of calculating the BPG was used. The density profile was that described in the first row in Table 2.

b. For all the experiments in this column, the hybrid BPG was not used because of an unresolved interface problem. For experiments 1 and 2, the density field was that described in the first row in Table 2; for experiment 3, the density field was that described in the second row of Table 2

For the conditions of the first experiment for the flat bottom domain, Luettich [19] derived an analytic solution for the surface elevation and east-west ("along-channel") velocity, as given below

$$\frac{\partial \zeta}{\partial x} = -\frac{h}{2}\frac{\partial \rho}{\partial x}\frac{\left(1 + \frac{kh}{4E_z}\right)}{\left(1 + \frac{kh}{3E_z}\right)} \tag{8}$$

$$u = -\frac{g}{6E_z}\frac{\partial \rho}{\partial x}\left(z^3 + \frac{h^3}{4}\right) + \frac{g}{2E_z}\frac{\partial \zeta}{\partial x}\left(z^2 - \frac{h^2}{3}\right) \tag{9}$$

where k is the slip condition, h is the bathymetry, z is the depth and E_z is the vertical eddy viscosity.

Results

BPG Tests

BPG results for all four methods matched the analytic solution for the flat bottom experiments of Table 2.

For the sloped bottom experiments of Table 2, representative results for the first experiment are shown in Figure 4 at two different vertical profiles (two

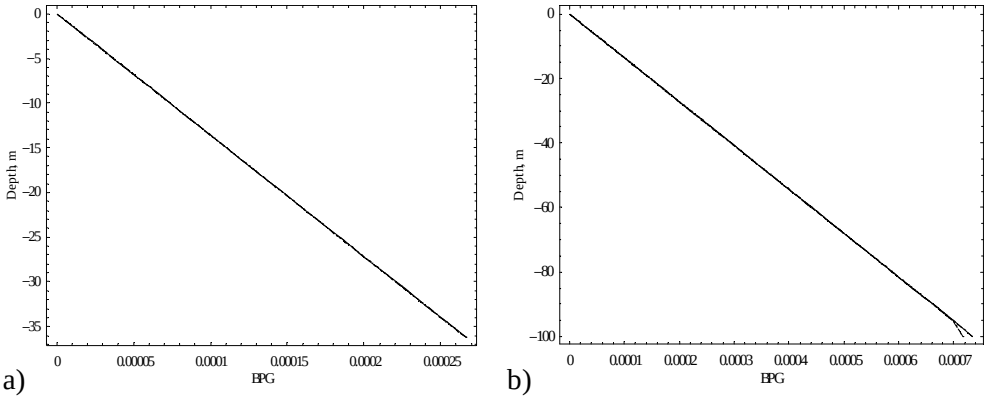

Figure 4. BPG vs. depth at two locations along the east-west axis; one near 35m depth (a) and one near 100 m depth (b). (dot dash = hybrid, long dash = quoddy, short dash = sigma, medium dash = adcirc, solid = analytic)

different locations in the domain). As can be seen, all four methods nearly match the analytic solution except for a slight tailing of the BPG near the bottom of the 100 m end of the domain for the hybrid and QUODDY methods.

Figure 5 shows the BPG results for the second sloped bottom experiment at

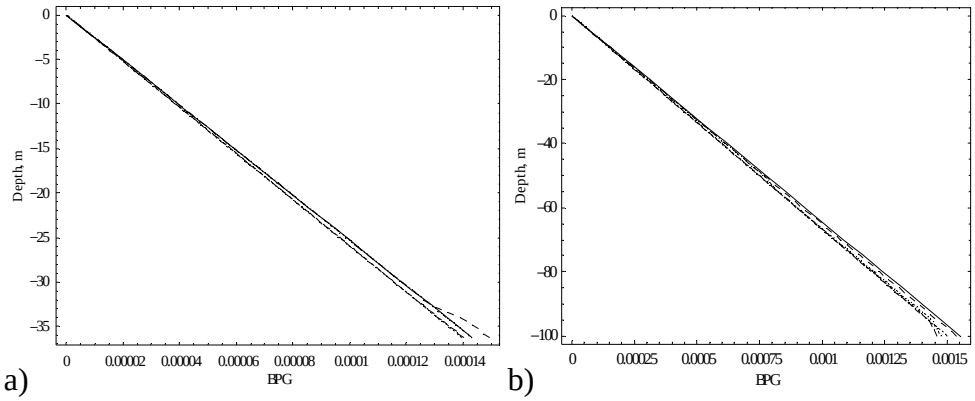

Figure 5. BPG vs. depth at two locations along the east-west axis; one near 35m depth (a) and one near 100 m depth (b). (dot dash = hybrid, long dash = quoddy, short dash = sigma, medium dash = adcirc, solid =

two different east-west locations. Again, all four methods produce acceptable results, but ADCIRC has a slight tail near the 35 m bottom. Figure 6 shows how the BPG compares to the analytic solution as one takes an east-west slice through the

domain at a constant 10 m depth. Again, results from all four methods are good.

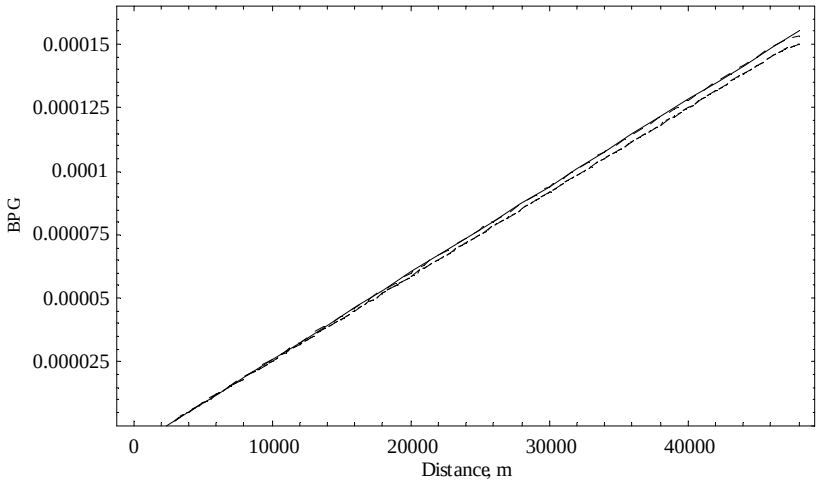

Figure 6. BPG vs. distance along the east-west direction at a depth of 10m. (dot dash = hybrid, long dash = quoddy, short dash = sigma, medium dash = adcirc, solid = analytic)

Figures 7 and 8 show the BPG results for the more complex density field (third sloped bottom experiment) where the "true" solution was obtained from an over-resolved grid (101 levels). Figure 7 illustrates the BPG vs. depth near the

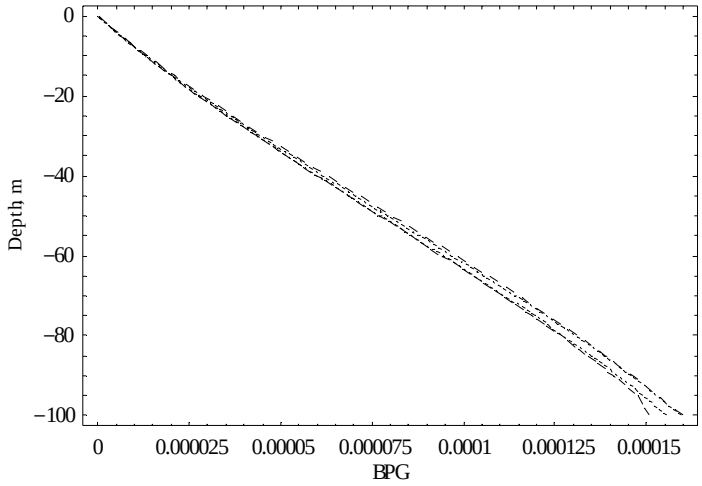

Figure 7. BPG vs. depth near the 100m (west) end of the domain. (dot dash = hybrid, long dash = quoddy, short dash = sigma, medium dash = adcirc, solid = "over-resolved")

100m end of the domain; Figure 8 illustrates the east-west BPG value along the 10m depth contour. Not shown on the figure is the hybrid scheme because it produced unrealistic results, a curious result since the method worked well in the other test

cases. The issue clearly needs further investigation.

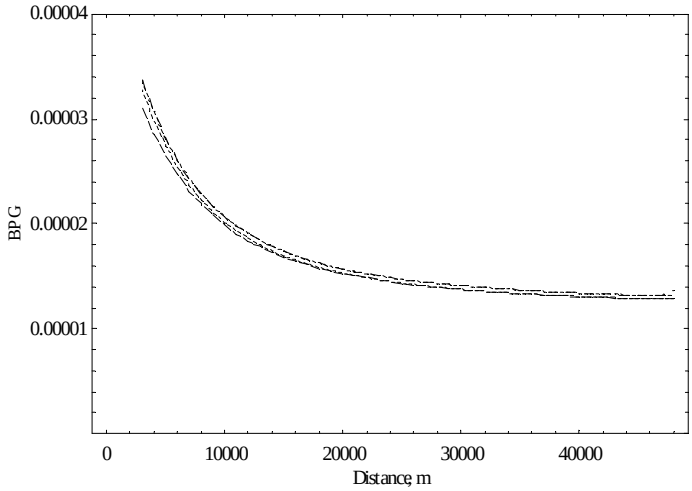

Figure 8. BPG vs. distance along the east-west direction at a depth of 10m. (long dash = quoddy, short dash = sigma, medium dash = adcirc, solid = "over-resolved")

For both the stratified (Table 2, #4) and the field (Table 2, #5) density profile, the analytic solution is zero BPG (because the horizontal gradient of density is zero). However, all three methods (hybrid not tested) produced similar results that showed zero or non-zero BPG's over much of the domain, but introduced a small fictional gradient over part of the domain. It appears that the fictional BPGs are independent of vertical resolution. Clearly, the numerical interpolation of the density field is smearing sharp interfaces so that the horizontal density gradient is not zero. We are investigating solutions to this problem but have no recommendations at this time. Based on Walters and Foreman's [32] work, additional horizontal resolution may help resolve this problem; such studies are part of our research outline.

Velocity Tests

Adequacy of the velocity model was tested by comparing the analytic results for the flat bottom domain, test case 1 (given by equations (8) and (9)) with the numerical results for 21 nodes. Figure 9 illustrates the results for both the 10m and 100m depths. As can be seen, the results match exactly. We do note that for this

simplified (and physically unrealistic) density field, the numerical and analytic

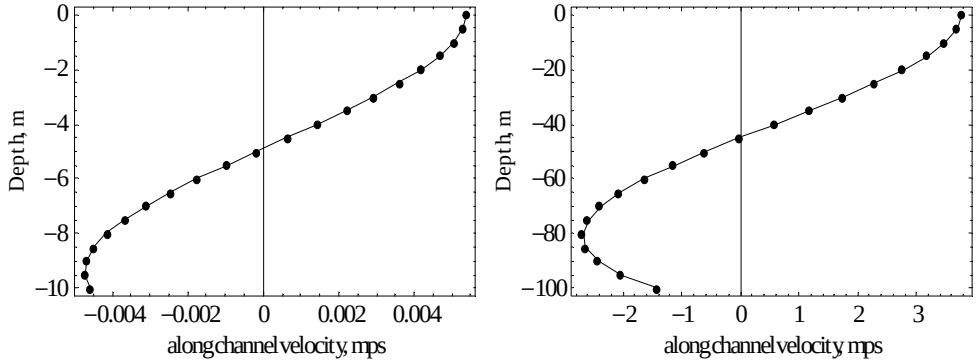

Figure 9. Comparison of the analytical (solid) and numerical (dots) velocity vs. depth for the 10m and 100m flat bottom problem (case 1 in Table 3).

results do not match up for depths greater than a couple of hundred meters. Our hypothesis is that the assumptions behind the simplified solution (e.g., no advective acceleration) breakdown because the velocities are on the order of 1000's of meters per second.

During the second study for the flat bottom problem, we found that the time to reach steady-state from a cold start was significantly reduced through the use of a ramp function (hyperbolic tangent) to slowly spin up the problem over a period of hours (e.g., a 0.25 day ramp for a 1 day simulation).

Results from the fourth flat bottom experiment are inconclusive because different east-west locations in the domain show different trends. In general, however, the no slip condition produces unrealistic results, while the linear slip produces the most qualitatively realistic results.

Our past work with the ADCIRC model [14] has shown that the "G" parameter has a significant impact of overall solution results. In particular, too low of a G-value leads to mass balance errors and errors in the generation of nonlinear constituents, while too high of a value leads to spurious $2\Delta x$ noise. For the conditions noted in the fifth line of Table 3, we varied G by several orders of magnitude above and below the base value. For the conditions specified, no impact on the vertical velocity profile was observed.

With regard to the sloped bottom problem, we note that for the first experiment of Table 3, results were qualitatively similar to the flat bottom case with the exception that the along-channel velocities were about 50% higher. This can be expected because of the deeper bathymetries (pressure due to density differences is accentuated).

The results of the second sloped bottom experiment were inconclusive (they either did not converge to a steady solution or varied unrealistically across the domain).

In the third sloped experiment of Table 3, one of the most notable observations is that the small differences in BPG (see Figures 7 and 8) manifested themselves as much larger differences in the vertical velocity profile.

Observations/Future Work

Results from this preliminary study suggest the following. Many of these results are expected or obvious and confirm what others have found in their studies; the ground work for the next, and more complex, round of testing is in place.

- A density gradient that increases linearly from 1036 kg/m^3 to 1000 kg/m^3 at the ends of the domain produces unrealistic along-channel velocities for depths greater than 100 m.
- Vertical refinement from 21 to 101 levels showed little to no improvement for the density gradients used in the test cases. However, we anticipate that this will become more of an issue when we simultaneously refine the horizontal grid and the density varies more dramatically, both vertically and horizontally, e.g., high density wedge on a slope.
- Interfaces can be smeared by numerical interpolation, which introduces small, fictional baroclinic pressure gradients.
- Use of a ramp function generates fewer oscillations at start-up.
- For the simplified test cases with the ideal basin, the complexity of the combined topography and density field is not great enough to trigger the instabilities that were observed in the Arabian Gulf simulation.

Acknowledgments

Funding is provided, in part, through the National Science Foundation, contract #ACI-9623592 and the University of Oklahoma. This work is partially supported through the Office of Naval Research's Navy Ocean Modeling and Prediction Program (Award Number N0001499WX30113).

References

1. Bijvelds, M.D.J.P, J. A. Th. M. Van Kester, and G. S. Stelling, "A Comparison of Two 3D Shallow Water Models Using Sigma-coordinates and z-coordinates in the Vertical Direction," *Estuary and Coastal Modeling 6,* Spaulding and Butler, eds., 130-147, ASCE, 1999.
2. Blain, C. A. "Barotropic Tidal and Residual Circulation in the Arabian Gulf", *Estuarine and Coastal Modeling, Proc. of the 5th International Conference*, ASCE, 166-180, 1998.
3. Blain, C. A., personal communication, June 2001.
4. CH3D, chl.wes.army.mil/software/ch3d.

5. Chippada S., C. Dawson, M. Martinez, M. Wheeler, "A Godunov-type Finite Volume Method for the System of Shallow Water Eqns", *Comp. M. in App. Mech. and Engr.*, 151(1-2), 105-131.
6. Dresback, K., R. Kolar, "An Implicit Time Marching Algorithm for Shallow Water Models Based on the GWC Equation," *Int'l J. Num. M. Fluids*, 36, 925-945, 2001.
7. Feyen J., J. Atkinson, J. Westerink, "Issues in Hurricane Surge Comp. Using a GWCE FE Model", *Comp. M. in Water Res. XIII*, Bentley et al. (eds.), Balkema, Rotterdam, 865-872, 2000.
8. Foreman, M., "A Comparison of Tidal Models for the Southwest Coast of Vancouver Island", *Comp. M. in Water Res.*, Celia et al. (eds.), Comp. Mech.s/Elsevier, Southampton, 231-236, 1988.
9. Fortunato A., A. Baptista, "Vertical Discretization in Tidal Flow Simulations", *Int'l J. Num. M. Fluids*, 1996, 22, 815-834.
10. Gray, W., "A Finite Element Study of Tidal Flow Data for the North Sea and English Channel", *Adv. Water Res.*, 12, 3:143-154, 1989.
11. Kinnmark, I., *The Shallow Water Wave Equations: Formulation, Analysis, and Application*, Lecture Notes in Engineering, No. 15, Springer-Verlag, 187 pp, 1986.
12. Kolar, R. and W. Gray, "Shallow Water Modeling in Small Water Bodies", *Comp.Meth. in Surface Hyd.*, Gambolati et al. (eds.), Comp. Mech./Springer-Verlag, 149-155, 1990.
13. Kolar, R., W. Gray, J. Westerink, R. Luettich, "Shallow Water Modeling in Spherical Coordinates: Eqn Formulation, Num. Implementation, and Application," *J. Hyd. Res.*, 32(1), 3-24, 1994.
14. Kolar, R. L., J. J. Westerink, M. E. Cantekin, and C. A. Blain, "Aspects of Nonlinear Simulations Using Shallow Water Models Based on the Wave Continuity Equation," *Computers and Fluids*, 23(3), 523-538, 1994.
15. Leendertse, J., "Aspects of a Computational Model for Long-Period Water Wave Propagation", Memorandum RM-5294-PR, Rand Corporation, 1967.
16. Luettich, R., J. Westerink, N. Scheffner, *ADCIRC. Report 1: Theory and Methodology of ADCIRC-2DDI and ADCIRC-3DL*. Technical Report DRP-92-6, USACE, Washington, DC, 1992.
17. Luettich, R., J. Westerink, *Implementation and Testing of Elemental Flooding and Drying in the ADCIRC Hydrodynamic Model*. Final Report, 8/95, Contract #DACW39-94-5689, 1995.
18. Luettich, R., J. Westerink, "Formulation and Numerical Implementation of the 3D ADCIRC Finite Element Model Version 36.01," internal report, 21 pp., 2001.
19. Luettich, R.A., Westerink, J.J., "Baroclinic Enhancements to the ADCIRC Finite Element Model Version 35.03,", UNC, Morehead City, NC, 1999.
20. Lynch, D., F. Werner, A. Figuerola, G. Parrilla, "Finite Element Modeling of Reduced-Gravity Flow in the Alboran Sea: Sensitivity Studies", *Proc.: Gibraltar Experiment*, Madrid, Spain, 1988.
21. Lynch, D., W. Gray, "A Wave Equation Model for Finite Element Tidal Computations", *Comp. and Fluids*, 7, 3:207-228, 1979.
22. Lynch, D., J. Ip, C. Naime, F. Werner, "Comprehensive Coastal Circulation Model with App. to the Gulf of Maine," *Cont. Shelf Res.*, 16(7), 875-906, 1996.
23. Mark, D., N. Scheffner, "Development of a Large Scale Tidal Circulation Model for

the Mediterranean, Adriatic and Aegean Seas", *4th ECM Proceedings,* ASCE, 168-179, 1996.
24. Martin, P. J., *Description of the Navy Coastal Ocean Model Version 1.0*, Technical Report NRL/FR/7322--00--9962, Dept. of the Navy, NRL, Stennis Space Center, MS, 2000.
25. Naimie, C., D. Lynch, "Applications of Nonlinear 3D Shallow Water Eqns to a Coastal Ocean", *Comp. M. in Water Res. IX*, Russell et al. (eds.) Comp. Mech./ Elsevier, London, 589-608, 1992.
26. Parr, V., J. Westerink, M. Wheeler, personal communication, 2001.
27. Partridge, P., C. Brebbia, "Quadratic Finite Elements in Shallow Water Problems", *J. Hydraulics Division, ASCE,* 102, HY9, 1299-1313, 1976.
28. Pickard, G.L. and W.J. Emery, *Descriptive Physical Oceanography: An Introduction*, Butterworth-Heinemann, 320 pp., 1990.
29. Platzman, G., "A Numerical Computation of Surge of 26 June 1954 on Lake Michigan", *Geophysics*, 6(3-4), 407-438, 1959.
30. Princeton Ocean Model (POM), www.aos.princeton.edu/wwwpublic/htdocs.pom.
31. Taylor, C., J. Davis, "Tidal and Long-Wave Propagation: A Finite Element Approach", *Computers and Fluids*, 3, 2-3:125-148, 1975.
32. Walters, R.A. and Foreman, M.G.G., "A 3D, Finite Element Model for Baroclinic Circulation on the Vancouver Island Continental Shelf," *Journal of Marine System*, 3, 1992, pp. 507-518.
33. Westerink J., R. Luettich, C. A. Blain, N. Scheffner, *ADCIRC. Report 2: Users Manual for ADCIRC-2DDI*, Department of the Army, USACE, Washington, DC, 1994.
34. Westerink, J., R. Luettich, A. Baptista, N. Scheffner, P. Farrar, "Tide and Storm Surge Predictions Using a Finite Element Model", *J. of Hydraulic Engineering*, 118, 1373-1390, 1992.